Bioactive Materials 22 (2023) 312–324

Contents lists available at ScienceDirect

Bioactive Materials

journal homepage: www.keaipublishing.com/en/journals/bioactive-materials

Enhancing cartilage repair with optimized supramolecular hydrogel-based scaffold and pulsed electromagnetic field

Yucong Li [a,1], Linlong Li [a,1], Ye Li [a,c,1], Lu Feng [a], Bin Wang [d], Ming Wang [a], Haixing Wang [a], Meiling Zhu [e], Yongkang Yang [a], Erik I. Waldorff [b], Nianli Zhang [b], Ingmar Viohl [b], Sien Lin [a], Liming Bian [f], Wayne Yuk-Wai Lee [a,g,**], Gang Li [a,*]

[a] Department of Orthopaedics & Traumatology, Stem Cells and Regenerative Medicine Laboratory, Li Ka Shing Institute of Health Sciences, The Chinese University of Hong Kong, Prince of Wales Hospital, Shatin, Hong Kong Special Administrative Region
[b] Research & Clinical Affairs, Orthofix Medical Inc., Lewisville, TX, USA
[c] Department of Rehabilitation Sciences, Hong Kong Polytechnic University, Hong Kong Special Administrative Region
[d] Innovation Centre for Advanced Interdisciplinary Medicine, Key Laboratory of Biological Targeting Diagnosis, Therapy and Rehabilitation of Guangdong Higher Education Institutes, The Fifth Affiliated Hospital of Guangzhou Medical University, Guangzhou, China
[e] The Eighth Affiliated Hospital, Sun Yat-Sen University, Shenzhen, PR China
[f] School of Biomedical Sciences and Engineering, National Engineering Research Center for Tissue Restoration and Reconstruction, Key Laboratory of Biomedical Materials and Engineering of the Ministry of Education, South China University of Technology, Guangzhou, PR China
[g] Department of Orthopaedics and Traumatology, SH Ho Scoliosis Research Laboratory, Joint Scoliosis Research Center of the Chinese University of Hong Kong and Nanjing University, The Chinese University of Hong Kong, Hong Kong Special Administrative Region

ARTICLE INFO

Keywords:
Supramolecular hydrogels
Pulsed electromagnetic field
Cartilage tissue engineering
Mesenchymal stem cells
Chondrogenesis

ABSTRACT

Functional tissue engineering strategies provide innovative approach for the repair and regeneration of damaged cartilage. Hydrogel is widely used because it could provide rapid defect filling and proper structure support, and is biocompatible for cell aggregation and matrix deposition. Efforts have been made to seek suitable scaffolds for cartilage tissue engineering. Here Alg-DA/Ac-β-CD/gelatin hydrogel was designed with the features of physical and chemical multiple crosslinking and self-healing properties. Gelation time, swelling ratio, biodegradability and biocompatibility of the hydrogels were systematically characterized, and the injectable self-healing adhesive hydrogel were demonstrated to exhibit ideal properties for cartilage repair. Furthermore, the new hydrogel design introduces a pre-gel state before photo-crosslinking, where increased viscosity and decreased fluidity allow the gel to remain in a semi-solid condition. This granted multiple administration routes to the hydrogels, which brings hydrogels the ability to adapt to complex clinical situations. Pulsed electromagnetic fields (PEMF) have been recognized as a promising solution to various health problems owing to their noninvasive properties and therapeutic potentials. PEMF treatment offers a better clinical outcome with fewer, if any, side effects, and wildly used in musculoskeletal tissue repair. Thereby we propose PEMF as an effective biophysical stimulation to be 4th key element in cartilage tissue engineering. In this study, the as-prepared Alg-DA/Ac-β-CD/gelatin hydrogels were utilized in the rat osteochondral defect model, and the potential application of PEMF in cartilage tissue engineering were investigated. PEMF treatment were proven to enhance the quality of engineered chondrogenic constructs *in vitro*, and facilitate chondrogenesis and cartilage repair *in vivo*. All of the results suggested that with the injectable self-healing adhesive hydrogel and PEMF treatment, this newly proposed tissue engineering strategy revealed superior clinical potential for cartilage defect treatment.

Peer review under responsibility of KeAi Communications Co., Ltd.

* Corresponding author. Department of Orthopaedic and Traumatology, Faculty of Medicine, The Chinese University of Hong Kong, Hong Kong Special Administrative Region.

** Corresponding author. Department of Orthopaedic and Traumatology, Faculty of Medicine, The Chinese University of Hong Kong, Hong Kong Special Administrative Region.

E-mail address: gangli@cuhk.edu.hk (G. Li).

[1] These authors contributed equally to this work.

https://doi.org/10.1016/j.bioactmat.2022.10.010
Received 24 June 2022; Received in revised form 5 October 2022; Accepted 5 October 2022
Available online 12 October 2022

1. Introduction

Due to the avascular nature, cartilage lacks innate self-repair ability to restore physiological structure and functions. Therefore, cartilage defect resulting from sudden injury or gradual wear and tear will eventually progress to osteoarthritis over time [1]. Current available treatments are mainly prescribed for symptoms relief only. Functional tissue engineering strategy using biomaterials has been proposed and actively investigated to provide innovative approach for the repair/regeneration of damaged cartilage.

Variety of natural and synthetic materials have been used as potential carrier biomaterials of cells or therapeutic agents for cartilage repair [2]. Hydrogels made of various polymers have been shown to promote the chondrogenesis and cartilage regeneration in the presence of inductive factors by providing the conducive 3D microenvironment [3,4].

Specially, hydrogels fabricated by natural polymers, such as hyaluronic acid (HA) [5–7], collagen [8], chitosan [9,10], and alginate [11], have been widely used as defect-filling treatments because of their biocompatibility, low immunogenicity, biodegradability, and suitable physical properties. Li et al. [7] prepared an in situ forming injectable hydrogel system composed of hyperbranched poly (ethylene glycol) (HB-PEG) and thiol-functionalized hyaluronic acid (HA-SH) crosslinked via thiol-ene reaction. The as-prepared hydrogels exhibited tunable and stable mechanical properties and rapid in situ gelation rate under physiological conditions. Besides, based on the HB-PEG, thiolated-chondroitin sulfate (CS-SH) was selected to fabricate CS-SH/HB-PEG hydrogels [12]. The prepared hydrogel exhibited rapid gelation, excellent mechanical properties and prolonged degradation properties.

In our previous work [13], an effective "Host-Guest Macromer" (HGM) approach for the preparation of supramolecular gelatin hydrogels was studied. The HGM hydrogels are self-healable, injectable, re-moldable and shows ideal mechanical properties due to the reversible nature of the host-guest interactions and chemically crosslinked acrylated structure. Herein, based on the previous study, we would like to introduce a modified hydrogel design by supplementing dopamine functionalized alginate (Alg-DA) to the original formula (photo--crosslinkable acrylated β-cyclodextrins (Ac-β-CDs) and gelatin). In this design, chemical and physical multiple crosslinking mechanisms were simultaneously incorporated into the hydrogel, including UV-induced covalent bonds, host-guest interactions, hydrogen bonding, and π-π aromatic stacking interactions (Fig. 1 a). Therefore, better physical properties could be achieved to better meet the complicated requirements in cartilage regeneration. The multi-crosslinked structure improves their injection abilities, mechanical performance, and better self-healing abilities, and further endows the hydrogel with new physical properties like suitable swelling ratio, appropriate degradation rate and tissue-adhesive ability. The new design introduces a pre-gel state during hydrogel preparation, where mixed solution exhibit increased viscosity, allowing the pre-gel to remain in a semi-solid condition (Figure S1 a). This pre-gel state before crosslinking granted more hydrogel administration routes, which brings hydrogels the ability to adapt to complex clinical scenarios (Fig. 1 b). Moreover, the catechol structure in dopamine can be oxidized into quinone or semi-quinone groups. The obtained quinone or semi-quinone structure could react with amino groups of the substrate by Schiff base reaction [14]. Thus, the integration between the hydrogels with host tissue could be effectively promoted, which could facilitate the healing process and recovery of its original function [15–17].

While suitable scaffolds can be designed, they cannot create high-quality cartilage tissue independently. The complicated requirements in cartilage regeneration often led to the failure of cartilage repair [18]. MSCs based stem cell therapy and tissue engineering strategy represent a promising solution. MSCs can differentiate into numerous cell types—including chondrocytes, fibrochondrocytes, and hypertrophic chondrocytes—resulting in a mixture of cartilaginous, fibrous, and hypertrophic tissues [19,20]. The success of MSC-based techniques may

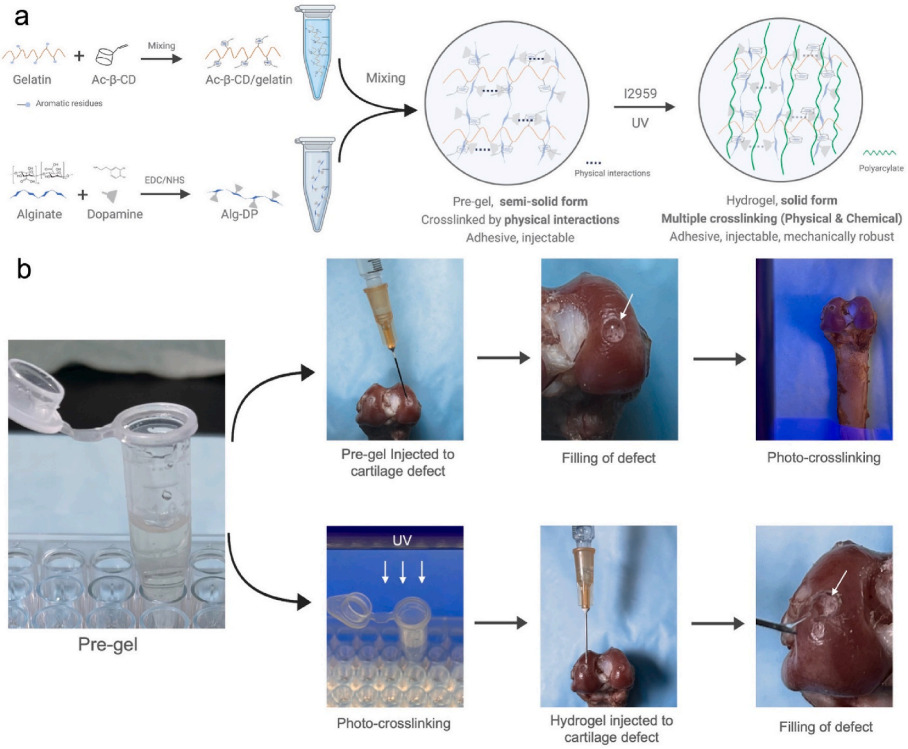

Fig. 1. a. Schematic illustration of the hydrogel design (*Created with* BioRender.com). b. Under pre-gel state, the mixed solution can be firstly injected to cartilage defect site, and then in situ crosslinked under UV exposure. Per-gel can also be photo-crosslinked first and injected to the defect site, the tissue-adhesive property allows the hydrogel to be tightly attached. Either way, smooth cartilage surface can be restored.

remain limited if the presence of fibrous and hypertrophic tissue cannot be eliminated. Therefore, biological augmentative strategies are urgently needed to improve the therapeutic outcomes of tissue engineering in cartilage repair. In orthopaedics field, previous studies have proposed "the diamond concept" [21], which embodies a 4th element, environmental biophysical stimulation, to underpin tissue engineering,. As a safe, noninvasive biophysical strategy with fewer, if any side effects for tissue repair, pulsed electromagnetic fields (PEMF) could not only benefits cartilage-related cells *in vitro* including promoting proliferation, increasing anabolic activities, and antagonizing the catabolic effects of inflammation [22–25], but also provide chondro-protective and chondro-regenerative effects on articular cartilage *in vivo* [26–29]. Therefore, we purpose that with the promising chondrogenic effects both *in vitro* and *in vivo*, PEMF could improve the quality of engineered biomaterial *in vitro*, and enhance cartilage repair *in vivo*, making it suitable as the 4th element in cartilage tissue engineering via augmenting the benefit of biomaterials consists of cells, scaffolds and bioactive factors.

In this study, we hypothesized that PEMF signal could benefit MSCs-based cartilage tissue engineering and promote cartilage repair/regeneration, and with Alg-DA/Ac-β-CD/gelatin hydrogel, we investigated the effects of PEMF stimulation on MSCs chondrogenesis *in vitro* and *in vivo*, and its effect on enhancing cartilage repair in combination of MSCs-based tissue engineering using a rat osteochondral defect model.

2. Methods

All experiments were approved by the Animal Research Ethics Committee of the Chinese University of Hong Kong (AEEC number:20-225-HMF).

2.1. Isolation of rat BMSCs and human BMSCs

Green fluorescent protein (GFP) Sprague-Dawley rats (male, 8 weeks, SD-Tg (CAG-EGFP) Cz-004Osb) were used for rat BMSCs (rBMSCs) isolation. rBMSCs were obtained from the bone marrow of GFP-SD rats by density gradient centrifugation (850×*g*, 20 min). Under the approval of IRB of author's institution (CREC Ref No. 2014.291-T), human BMSCs (hBMSCs) from three patients with osteoarthritis (OA) and undergoing total knee replacement surgery were obtained as previous described [30]. The obtained cells were cultured in α-modified Eagle's medium (αMEM, Gibco, ThermoFisher Scientific, USA) supplemented with 10% fetal bovine serum (FBS, Gibco, ThermoFisher Scientific, USA) and 1% penicillin/streptomycin (PS, Gibco, ThermoFisher Scientific, USA) (500 cells/cm^2, 37 °C, 5% CO_2) to isolate BMSCs and form colonies; medium was changed every 3 days. Cells at passage 3–5 were used for all following experiments.

2.2. Hydrogel preparation

2.2.1. Materials

All the reagents including sodium alginate (Alg), dopamine hydrochloride (DA), 1-(3-Dimethylaminopropyl)-3-ethylcarbodiimide hydrochloride (EDC·HCl), N-hydroxysuccinimide (NHS) and 2-hydroxy-4′-(2-hydroxyethoxy)-2-methylpropiophenone (Irgacure 2959) were purchased from Shanghai Aladdin Biochemical Technology Co., Ltd. The water used in the experiments was purified using Millipore Milli-Q Ultrapure water systems.

2.2.2. Synthesis and characterization of dopamine-modified alginate (Alg-DA)

2.0 g of Sodium alginate (10.1 mmol, according to the repeating unit of alginate molecule) was added into 200 mL of Milli-Q water and stirred until fully dissolved. Then EDC·HCl (1.936 g, 10.1 mmol) and NHS (1.162 g, 10.1 mmol) were added in the above alginate solution. The reaction solution was stirred for 60 min at room temperature. During this procedure, the carboxylic groups in the alginate molecules would be fully activated. After that, different amounts (0.639 g, 0.958 g, 1.915 g) of dopamine (3.37, 5.05, 10.1 mmol) were added into the above reaction solution and stirred for another 12 h at room temperature under N_2 atmosphere. Then, the reaction solution was dialyzed (MWCO 3500) against distilled water (pH 6) three days and the water was changed twice a day. Then the dialyzed materials solution was lyophilized. The corresponding product dopamine-modified alginate was denoted as Alg-DA-1, Alg-DA-2 and Alg-DA-3.

The successful preparation of synthesized Alg-DA was confirmed by nuclear magnetic resonance (^{1}H NMR) spectroscopy, which was performed through a Bruker 500 MHz NMR spectrometer (Bruker BioSpin GmbH). The samples were dissolved into D2O at a concentration of 10 mg/mL before the test.

The degree of dopamine substitution of different groups of Alg-DA was determined by measuring the absorbance at 280 nm using an ultraviolet–visible (UV–vis) spectrophotometer and calculating from a standard curve of dopamine hydrochloride solution. Different groups of Alg-DA solution were prepared with the concentration of 1 mg/mL and used as the tested samples. Dopamine hydrochloride solution was used to generate a standard curve with the concentrations ranging from 0.0156 to 1 mg/mL.

2.2.3. Synthesis of acrylated β-cyclodextrins (Ac-β-CD)

The Ac-β-CD was synthesized and obtained according to our previous study [31].

2.2.4. Preparation of Alg/Ac-β-CD/gelatin and Alg-DA/Ac-β-CD/gelatin hydrogel

Firstly, gelatin was dissolved into dH_2O at 37 °C with fixed concentration of 5% (w/V). For the preparation of Alg/Ac-β-CD/gelatin hydrogel, 5 wt% of Ac-β-CD were added into gelatin solution under continuous stirring. After 20 min, 1% of Alg was added into the solution and thoroughly stirred. Then the initiator Irgacure 2959 was added at a concentration of 0.05% (w/V). The mixture was thoroughly stirred at 37 °C and a homogenous solution was obtained. The pH of the solution was kept at 7.2. Then the pre-gel solution was transferred into cell culture plate. Then 365 nm ultraviolet (UV) light (10 mW/cm^2) was utilized to prepare the Alg/Ac-β-CD/gelatin hydrogels. For the preparation of Alg-DA/Ac-β-CD/gelatin hydrogel, the procedure was almost the same as above, except that the 1 wt% of Alg-DA was added instead of Alg.

2.3. Hydrogel swelling analysis

To evaluate the hydrogel swelling property, the prepared different groups of Alg/Ac-β-CD/gelatin hydrogels and Alg-DA/Ac-β-CD/gelatin hydrogels (500 μL of pre-gel solution for one sample) were lyophilized and then weighed to determine the dry weight of hydrogel material (W_0). Then the samples were incubated in PBS at 37 °C for 24 h to determine the water swelling degree. At different time points, the tested samples were taken out and the residual PBS on the sample surface was carefully removed, and the weight of the samples was recorded (W_t). After the test, the swelling ratio (SR) was calculated as the ratio of the weight of water in the swollen hydrogel at different time points to the weight of dry hydrogel: $SR = (W_t - W_0)/W_0$.

2.4. In vitro hydrogel degradation test

In vitro degradability of the Alg/Ac-β-CD/gelatin hydrogel and Alg-DA/Ac-β-CD/gelatin hydrogel was determined by weight changes of the hydrogels after incubated in PBS or Collagenase Type-I/PBS (0.1 mg/mL) at 37 °C for different time. The prepared different groups of Alg/Ac-β-CD/gelatin hydrogels and Alg-DA/Ac-β-CD/gelatin hydrogels (500 μL of pre-gel solution for one sample) were lyophilized and then weighed to determine the dry weight of hydrogel material (W_0). After that, the dried

hydrogel samples were immersed into PBS at 37 °C for 12 h for water equilibrium. Then the degradation test was conducted. The samples were removed from the incubation solution at different time of incubation. After carefully and thoroughly washing with distilled water, the samples were lyophilized and weighed (W_t). Degradation rate (DR) of the hydrogel samples was calculated in terms of the following equation, $DR = (W_0\text{-}W_t)/W_0 \times 100\%$.

2.5. Adhesion property

The adhesive properties of the as-prepared hydrogels were determined through the lap-shear adhesion measurements. By placing the hydrogel between two glass slides with the overlapped contact area dimensions of 25 mm × 20 mm x 0.5 mm, the samples were pressed slightly for 10 s to enhance the adhesion. Then the test samples were kept in 37 °C incubator for 12 h. Subsequently, the samples were pulled to failure and the max load was measured.

2.6. Induction of chondrogenic differentiation of MSCs-laden hydrogels and PEMF exposure in vitro

The therapeutic PEMF signal used in this study is designed by Orthofix Medical Inc. (Physio Signal, 10T/s, 15 Hz, Orthofix Medical Inc, USA). As demonstrated in our previous study [32], our signal is safe and effective, and has been approved by FDA to manage long bone nonunions [33]. To investigate the effects of PEMF signal on chondrogenic differentiation of BMSCs in 3D culture environment, rBMSCs-laden hydrogels were divided into two groups. PEMF group received daily PEMF treatment 3 h s/day for 21 days, and control group received no PEMF treatment. On day 0, rBMSCs-laden hydrogels were cultured in chondrogenic inductive medium (CIM, ThermoFisher Scientific, A1007101), and daily PEMF treatment (3 h s/day) was given to the cells using an *in vitro* PEMF device (Orthofix Medical Inc.). Control group was kept under the same conditions without PEMF exposure. Samples were collected on day 7, 14, and 21 (n = 6 per group per time point), cut into two equal parts. One half was subjected to RNA extraction for quantitative real-time PCR analysis (n = 4/group/time point.), and the other half was fixed with 4% paraformaldehyde (PFA) following alcian blue, safranin O and immunohistochemistry staining (n = 4/group/time point.).

2.7. Nude mice transplantation

rBMSCs-laden hydrogels prepared as previous described were cultured in CIM for 14 days. Nude mice (male, 8 weeks old) were randomly divided into two groups: Hydrogel and hydrogel + PEMF. Hydrogels were transplanted subcutaneously into the back of nude mice according to the grouping, and daily PEMF treatment (3 h s/day) were given to hydrogel + PEMF group via a specialized *in vivo* PEMF device (Orthofix Medical Inc.) [34]. The hydrogel group received no PEMF treatment. After 14 days of PEMF exposure, fresh samples were harvested for the mechanical test (n = 8). Other samples were cut into two halves. One half was subjected to RNA extraction for quantitative real-time PCR analysis (n = 8), and the other was fixed with 4% PFA following alcian blue, safranin O and immunohistochemistry staining (n = 8).

2.8. RNA-sequencing and bio-informatic analysis

hBMSCs were cultured in αMEM containing 10% fetal bovine serum and 100 U/mL penicillin with or without daily PEMF treatments (3 h s/day) for 7 days. Samples were then collected, and total RNA were extracted using RNeasy Mini Kit (Qiagen, Hilden, Germany). Total RNA was processed by mRNA enrichment method. The constructed DNA library was prepared as previously published [35], and RNA-sequencing was performed with BGISEQ-500 platform (Beijing Genomics Institute, Shenzhen, China) and hg38 genome database.

Differentially expressed genes (DEGs) were identified from RNA-seq data using an R package as previously described [36]. DEGs were defined as fold change ⩾2 and Q-value ⩽ 0.001. Kyoto Encyclopedia of Genes and Genomes (KEGG) pathway enrichment analysis was performed using DAVID (https://david.ncifcrf.gov). Candidate DEG functions and pathway interactions were analyzed using t the ClueGO plug-in of Cytoscape.

2.9. Validation and pharmacological inhibition study of ERK and p38 pathways

After bioinformatics analysis and literature review, ERK and p38-MAPK pathways were located as possible pathways mediating the effects of PEMF on hBMSCs chondrogenesis. To further validate the involvement of ERK and p38-MAPK pathways on chondrogenic differentiation of hBMSCs during PEMF treatments, on day 0, cell pellets were cultured in CIM and received daily PEMF treatment (3 h s/day) for 10 days. Cell pellets from control group were kept at same condition and received no PEMF treatment. Samples were collected on day 1, 3, 7 and 10 and subject to Western blot to analyze the expression and phosphorylation of ERK1/2 and p38 protein.

Pharmacological inhibition study was deployed to investigate the correlation between regulation of ERK and p-38 by PEMF treatment and chondrogenesis of hBMSCs. On day 0, Specific inhibitors of MEK / ERK (PD98059, 10 μmol/L, Invitrogen™, ThermoFisher Scientific, USA)), p38 (SB20350, 3 μmol/L, Sigma-Aldrich, USA), or a combination of both inhibitors were added into CIM of pellet culture, and cell pellets received daily PEMF treatment (3 h s/day) for 14 days. Samples were collected on day 1 to exam ERK1/2 and p38 activities after pharmacological inhibition through Western blot, and collected on day 7 and 14 for qPCR analysis of chondrogenic marker (*Sox9*) and hypertrophic marker (*RUNX2*).

2.10. Implantation of hydrogel into rat model of osteochondral defect

Three-month-old SD rats (male, weight 250–300 g, n = 40) were divided into 4 groups (n = 10), and the detailed experimental groups are shown in Table 1.

In brief, rat osteochondral defect models were established as previously described [37], and according to different groups, the osteochondral defects were transplanted with three types of hydrogels: blank hydrogels with no cells implanted, rBMSCs-laden hydrogels, and rBMSCs-laden hydrogels (Cells treated with daily 3 h PEMF *in vitro* exposure for 14 days), respectively. The osteochondral defects were created using a 1.5 mm diameter dental drill in the center of the femoral trochlear groove with 1.5 mm in depth. The defect was rinsed with 0.9% saline and the debris was removed using a curette. The defects were implanted with different biomaterials according to Table 1. Briefly, the pre-gel solution of Alg/Ac-β-CD/gelatin with initiator Irgacure 2959 was injected into the defects. Then 365 nm ultraviolet UV light (10 mW/cm^2) was utilized to initiate the gelation. Daily PEMF treatment of 3 h/day was given to the rats 24 h after surgery until termination. Rats were terminated after 8 weeks with pentobarbital overdose. The right femur of the rats was collected and were fixed in 10% buffered formalin.

Table 1
Detailed experimental groups of osteochondral defects repair.

Group	Material implanted	PEMF treatment after implantation
Blank	Blank hydrogels (no cells)	No PEMF treatment
MSCs	rBMSCs-laden hydrogels	No PEMF treatment
P-MSCs	PEMF enhanced rBMSCs-laden hydrogels	No PEMF treatment
P-MSCs + PEMF	PEMF enhanced rBMSCs-laden hydrogels	Daily PEMF treatment, 3 h/day

Samples were decalcified in a 10% solution of buffered ethylenediaminetetraacetic acid (EDTA, Sigma-Aldrich, USA). Histological and immunohistochemical staining were performed to determine the healing outcome of osteochondral defect.

2.11. In vivo PEMF exposure

For *in vivo* PEMF treatment, nude mice or rats were placed in plastic cages for PEMF exposure to eliminate interference by metal components and placed into the *in vivo* PEMF system (Orthofix Medical Inc.). Same PEMF signal used *in vitro* was applied to the animals. Daily PEMF treatment of 3 h/day was given to the animals as described above. Nude mice or rats placed under the same condition but without PEMF exposure served as the control group.

2.12. Quantitative real-time PCR

Total cellular RNA was extracted from hydrogel samples with MiniBEST universal RNA extraction kit (Takara, Japan), and reversely transcribed into cDNA with M-MLV reverse transcriptase according to the manufacturer's instructions (Takara, Japan). Real-time PCR was performed using the Step One Plus Real-Time PCR System (Applied Biosystems, USA). 10 μl reaction volume was consisted of 1 μl cDNA template diluted with Milli-Q water, 5 μl SYBR-Green Master Mix (2X, Applied Biosystems, USA), 3.4 μl PCR grade water, and 0.6 μl of primer (10 μM). The amplification procedure was carried out as follows: first at 95 °C for 5 min, and then 40 cycles of 95 °C for 15 s and 60 °C for 60 s. Primer sequences were shown in Table 2. The relative quantification of gene expression was analyzed with the values of $2^{-\Delta\Delta CT}$, normalized to the *GAPDH* expression.

2.13. Western blot

The cell pellets were collected and lysed using 50 μL radioimmunoprecipitation assay (RIPA) lysis buffer (Sigma-Aldrich, USA) with 1 mM phenylmethylsulfonyl fluoride (Roche, USA) at indicated time points. The lysate was centrifuged at 14 000 g for 15 min, supernatant collected and quantified using BCA assay kit (Thermo Fisher Scientific, USA). Normalized proteins were subject electrophoresis and electroblotted and probed with primary antibodies include ERK1/2 monoclonal antibody (1:1000, 13–6200, Sigma-Aldrich, USA), rabbit monoclonal anti-p-ERK1/2 (1:3000, ab184699, Abcam, UK), rabbit monoclonal anti-p38 (1:1000, ab170099, Abcam, UK), rabbit monoclonal anti-p-p38 (1:1000, ab4822, Abcam, UK) and mouse monoclonal anti-β-actin (1:1000, ab8226, Abcam, UK), overnight at 4 °C. Blots were then incubated with horseradish peroxidase (HRP)- conjugated secondary antibody (diluted 1:5000; Santa Cruz, CA, USA) at 37 °C for 1 h, and visualized using an ECL system (Millipore, Billerica, MA, USA), Optical intensity of each band were analyzed using ImageJ, and band intensity ratio ($A_{p\text{-}ERK}$ / A_{ERK} and $A_{p\text{-}p38}$ / A_{p38}) were used for data analysis.

2.14. Mechanical test

Mechanical test was performed as previous described to obtain the compression Young's modulus and ultimate strength [38]. Stress-relaxation analysis was conducted with MACH-1™ Mechanical Testing System (Biomomentum). The equilibrium Young's modulus was calculated by the MACH-1 Analysis software (Biomomentum, Laval) with the obtained equilibrium load after 1000 s of relaxation at 50% strain under uniaxial and unconfined compression.

2.15. Safranin O & fast green staining

After deparaffinized and hydrated, sections of samples were stained with 0.05% fast green (Sigma-Aldrich) solution for 5 min. Sections were rinsed with 1% acetic acid solution for 15 s and stained with 0.1% safranin O (Sigma- Aldrich) solution for 5 min. Residual dye was removed using 95% ethanol and absolute ethanol for 2 min each.

2.16. Histology and immunohistochemistry staining

After deparaffinization, H&E staining was performed on rat cartilage sections, and immunohistochemistry staining was performed on hydrogel sections and rat cartilage sections. Immunohistochemistry staining was performed using a standard protocol as previously reported [39]. Sections were incubated with primary antibodies to mouse anti-rat Collagen type II (Col II; ab34712, 1:100, Abcam, UK), rabbit anti-rat Collagen type X (Col X; ab58632, 1:200, Abcam, UK) or rabbit anti-rat MMP13 (MMP13; ab39012, 1:200, Abcam) overnight at 4 °C; a horseradish peroxidase-streptavidin detection system (Dako, USA) was used, followed by counterstaining with hematoxylin. ImageJ was used to analyze percentage of positive area in the hydrogel samples or cartilage defect sites. For hydrogel samples, five randomly selected pictures from each section taken at 400 × magnification were used for semi-quantitative analysis.

2.17. Cartilage repair analysis by the Wakitani scoring system

Rat cartilage sections of each defect at week 8 after hydrogel implantation were scored using H&E staining together with IHC staining of Col II to define the region of cartilage in newly formed surface tissue (n = 10 per group). Histology sections were blindly scored by three independent researchers based on a previously established scoring system by Wakitani et al. [40].

Table 2
Primers for quantitative real-time reaction (qPCR).

Gene Name	Forward (5′–3′)	Reverse (5′–3′)
Rat primers		
GAPDH	AGCCCAGAACATCATCCCTG	CACCACCTTCTTGATGTCATC
Sox-9	AGAGCGTTGCTCGGAACTGT	TCCTGGACCGAAACTGGTAAA
Col 2a1	AACCCAAAGGACCCAAATAC	CCGGACTGTGAGGTTAGGAT
ACAN	TTGTGACTCTGCGGGTCATC	GTCCCTAGGAGGGCCTTCAG
MMP13	AGGCCTTCAGAAAAGCCTTC	GAGCTGCTTGTCCAGGTTTC
Col 10a1	ATATCCTGGGGATCCAGGTC	TCCAGGTTCACCTCTTGGAC
Runx2	GAACCAAGAAGGCACAGAC	AATGCGCCCTAAATCACTG
Human primers		
Sox-9	TGGGCAAGCTCTGGAGACTTC	ATCCGGGTGGTCCTTCTTGTG
Runx2	GACAAGCACAAGTAAATCATTGAACTACAG	GTAAGGCTGGTTGGTTAAGAATCTCTG

GAPDH: glyceraldehyde-3-phosphate dehydrogenase, *Sox-9*: SRY (Sex-Determining Region Y)-box transcription factor 9, *Col 2a1*: Collagen type II alpha 1 chain, *ACAN*: Aggrecan, *MMP13*: Matrix metallopeptidase 13, *Col 10a1*: Collagen type X alpha 1 chain, *Runx2*: Runt-related transcription factor 2.

2.18. Statistical analysis

Data was presented as mean ± standard deviation. All the quantitative and semi-quantitative data were analyzed using SPSS 18.0 software for windows (SPSS, Chicago, IL, USA). Parameters were analyzed by analysis of variance (ANOVA). One-way ANOVA and Tukey multiple comparison was used for comparison among groups and two-way ANOVA and Tukey multiple comparison was used for comparison among groups and time factor. $p < 0.05$ was considered as statistically significant.

3. Results

3.1. Characterizations of Alg-DA and gelation of Alg/Ac-β-CD/gelatin and Alg-DA/Ac-β-CD/gelatin hydrogels

To fabricate the supramolecular Alg-DA/Ac-β-CD/gelatin hydrogels, Alg-DA was firstly prepared. The ^{1}H NMR spectra of the synthesized Alg-DA was presented in Supplementary Fig. S3. The results clearly showed the peaks at δ2.7–3.2, which were attributed to the $–CH_2-CH_2-$ groups of dopamine, and peaks at δ6.6–6.9 ppm, which were attributed to the phenyl groups of dopamine. The results indicated that dopamine was successfully grafted to the alginate. To determine the conjugation efficiency of the dopamine substitution reaction, UV–vis spectra were utilized. First, a standard curve of absorbance at 280 nm of a series of preset dopamine concentrations was obtained. And the absorbance of 1 mg/mL dopamine modified alginate was also measured. Through the standard curve, the concentration of catechol in the Alg-DA sample solution could be calculated. And the amount of alginate in the sample solution is a fixed value. Thus, 6.7%, 9.4 and 15.3% of the alginate molecule units of Alg-DA-1, -2 and -3 were conjugated with catechol according to this calculation.

The gelation time of each group of hydrogels was monitored by the inverted vial method. Under UV irradiation, the gelation time of each group of hydrogels was recorded when the pre-gel solution transferred to solid-like state. The gelation time of all the groups was about 15–20 min, and the substitution degree of dopamine had no obvious influence on the gelation time.

As our hydrogel design was successfully carried out, the hydrogels demonstrated ideal physical properties (Fig. 1, Fig. S1.b, Video 1), owning to the chemical and physical multiple crosslinking and interactions during gelation. Along with the enhanced physical properties, the Alg-DA/Ac-β-CD/gelatin hydrogels were injectable through a 23G needle, and self-healable and re-moldable after injection (Video 1). It is also noteworthy that our design introduced a pre-gel state. By simply mixing the Alg-DA with Ac-β-CD/gelatin solution, the physical interactions are readily formed, resulting in increased viscosity and limited fluidity of the pre-gel (Fig. S1a). Subsequent UV initiated polymerization of Ac-β-CD, resulting in the gelation of Alg-DA/Ac-β-CD/gelatin hydrogels that are more stable, physically strong, and mechanically robust.

Supplementary video related to this article can be found at https://doi.org/10.1016/j.bioactmat.2022.10.010

3.2. Hydrogel swelling test

The hydrogel swelling properties of the as-prepared hydrogels were determined through measuring the water uptake capacity. The swelling ratios of the Alg/Ac-β-CD/gelatin and Alg-DA/Ac-β-CD/gelatin hydrogels were monitored at 37 °C for 24 h. As shown in Fig. 2 a, all groups of hydrogels showed gradually increased swelling ratios within 2 h of incubation, and then the swelling ratios tended to be stable. Compared to unmodified group of hydrogels, all Alg-DA/Ac-β-CD/gelatin hydrogels showed decreased swelling ratio. And the Alg-DA-3/Ac-β-CD/gelatin hydrogel showed a lower swelling ratio of 9.62, which indicated that the swelling ratio of the hydrogel decreased because of the dopamine units

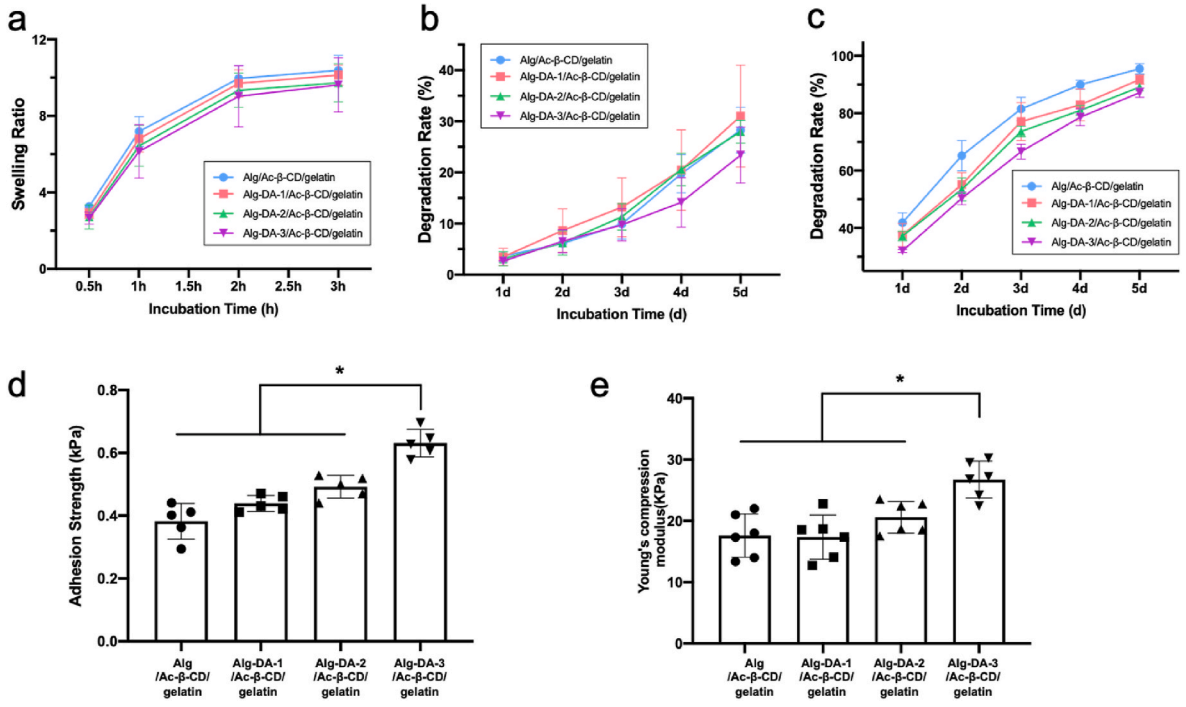

Fig. 2. Physical properties of the Alg/Ac-β-CD/gelatin and Alg-DA/Ac-β-CD/gelatin hydrogels
a Swelling behavior of Alg/Ac-β-CD/gelatin hydrogel and Alg-DA/Ac-β-CD/gelatin hydrogels with different dopamine grafting ratios incubated in PBS solution (n = 4/group). b and c. *In vitro* degradation properties of Alg/Ac-β-CD/gelatin hydrogel and Alg-DA/Ac-β-CD/gelatin hydrogels with different dopamine grafting ratios incubated in PBS solution (b) and Type-I collagenase/PBS (0.1 mg/mL) (c) (n = 4/group). d. Adhesion properties of Alg/Ac-β-CD/gelatin hydrogel and Alg-DA/Ac-β-CD/gelatin hydrogels with different dopamine grafting ratios through lap-shear adhesion test (n = 5/group). e. Young's compression modulus of Alg/Ac-β-CD/gelatin hydrogel and Alg-DA/Ac-β-CD/gelatin hydrogels with different dopamine grafting ratios (n = 6/group). *$p < 0.05$.

in the hydrogel system. Besides, as shown in Fig. S1 c, the volume of all groups of hydrogels slightly increased during the incubation, thus, the hydrogel could be implanted into defect area without obvious variation of volume.

3.3. In vitro degradation test

The implanted hydrogels are usually required to degrade properly for new tissue ingrowth, achieving a better regeneration of defect tissue. Thus, degradability is an important factor for the implanted hydrogels. In this study, biodegradation behaviors of the prepared hydrogels were measured in PBS and Type-I collagenase/PBS (0.1 mg/mL) solution at 37 °C for 5 days. Degradation test of the samples were conducted by measuring the weight loss during the incubation using a precision analytical balance. As shown in Fig. 2 b, the Alg/Ac-β-CD/gelatin hydrogel group incubated in PBS exhibited an approximate 3.62% of degradation rate after 1 d of incubation and differences between any two groups are not obvious. After 5 days of incubation, Alg-DA-3/Ac-β-CD/gelatin hydrogel showed a relative lower degradation rate. For the Alg/Ac-β-CD/gelatin hydrogel group incubated in Type-I collagenase/PBS (Fig. 2 c), 41.87% of the samples degraded after 1 d of incubation. With the incubation time increasing, the degradation rate gradually increased. And with the increasing of dopamine substitution ratio, the degradation rates of the hydrogels were reduced. After 5 days of incubation in Type-I collagenase/PBS, the degradation rate of Alg-DA-3/Ac-β-CD/gelatin hydrogel was 87.18%, which was the lowest among others. For the Alg-DA/Ac-β-CD/gelatin hydrogels, the relative low degradation rates might because of the introduced interactions of catechol groups in the Alg-DA.

3.4. Adhesion property and mechanical property

The adhesive tests were evaluated by placing the hydrogel between two glass slides based on the lap-shear stress test. As shown in Fig. 2 d, after the dopamine substitution, the Alg-DA/Ac-β-CD/gelatin hydrogels with different catechol grafting ratios displayed improved adhesion properties compared with the Alg/Ac-β-CD/gelatin hydrogels. Results showed that Alg-DA-3/Ac-β-CD/gelatin hydrogels showed the adhesion strength of 0.631 ± 0.044 kPa, which was significantly higher than other groups of hydrogels. The compression test results (Fig. 2 e) showed that the elasticity by compression was also improved by dopamine substitution. Alg-DA-3/Ac-β-CD/gelatin hydrogels showed Young's compression modulus of 26.478 ± 2.846 kPa, which was significantly higher than other groups of hydrogels.

3.5. Effects of PEMFs on rBMSCs chondrogenic and hypertrophic gene expression in vitro

Gene expression level of chondrogenic markers *SOX9*, *Col2a1*, *ACAN* and hypertrophic markers *MMP13*, *Col10a1*, *RUNX2* (Fig. 3 a) was detected by qPCR after chondrogenic differentiation for 7, 14, and 21 days in hydrogels. Our results showed that PEMF significantly upregulated the expression of chondrogenic mRNA, and downregulated the expression level of *RUNX2*.

Safranin O staining (Fig. 3 b) and immunohistochemistry (Fig. 3 c, d, e) staining demonstrated that PEMF promoted chondrogenic ECM formation starting from day 7. Significantly larger amounts of chondrogenic matrix were found in the PEMF group compared to control group. IHC staining of MMP13 and Col X (Fig. 3 d, e) showed PEMF treatment significantly inhibited formation of MMP13 and Col X. Staining results also demonstrated that hydrogel showed excellent properties for matrix deposition and cells aggregation. Newly synthesized matrix started to penetrate inside the hydrogels from day 7 and large scale of cell aggregation was observed inside the hydrogels starting from day 14.

3.6. Effects of PEMFs on MSCs chondrogenic and hypertrophic gene expression and ECM formation in vivo

After nude mice transplantation for 14 days, gross view of recovered hydrogels indicated that our hydrogels were highly deformable (Fig. 4 a). Volume of hydrogels in both groups was decreased compared to those before implantation (Average 31.9 ± 5.46 μL in control group, 30.4 ± 2.72 μL in PEMF group, initial volume before implantation: 50 μL), indicating that our hydrogels slowly degraded after implanted *in vivo* (Fig. 4 c). However, weight and density of the hydrogels were both increased after implantation, indicating that our hydrogels facilitated the large scale of ECM formation and deposition during implantation *in vivo*. Significantly higher weight and density of hydrogels were found in PEMF groups, indicating that PEMF treatment promoted ECM deposition. In comparison between control and PEMF groups, mechanical test demonstrated that significantly higher Young's modulus and ultimate strength were observed in PEMF group, likely resulted by the enhanced ECM formation from PEMF treatment (Fig. 4 d).

qPCR and staining were performed to determine mRNA expression level (Fig. 4 e) and ECM formation (Fig. 4 b, f, g and h) of the hydrogels. In consistent with *in vitro* results, qPCR and staining results showed that PEMF significantly promoted the gene expression and protein formation of chondrogenic markers and downregulated the expression of hypertrophic markers. Results indicate that PEMF treatment could provide chondro-inductive effects as well as chondroprotective potential during chondrogenesis.

3.7. Bioinformatic analysis of RNA-sequencing and validation study

To better understand the biological mechanisms associated PEMF treatments, hBMSCs from three patients were subject to RNA-sequencing with or without 7 days of PEMF exposure. 17388 transcripts were detected and analyzed, and among which, 54 DEGs (Fold change>2, $P < 0.05$) were identified. To further investigate the mechanism dictating the effects of PEMF on BMSCs, KEGG pathway enrichment analysis was performed. The top KEGG pathways were selected based on the most significant fold enrichment (Fig. 5 a, b). The gene-pathway interactions were further visualized in Cerebral Layout using ClueGo (Fig. 5 c). From the bioinformatic analysis, and in combination with the effects observed *in vitro* and *in vivo*, we found TNF-α signaling pathway as a potential target pathway in PEMF treatment.

To investigate TNF-α signaling pathway was involved in the effects of PEMF treatment, we visualized the gene expression changes of cells from three individual donors in KEGG pathview [41,42] (Fig. 5 d). From there, we identified that the two most important MAP kinases, extracellular signal-regulated protein kinase (ERK) and p38 kinase, were most likely to be the key factor of PEMF effects. Further validation using Western blot was performed (Fig. 5 e, f). Results showed that after chondrogenic induction without PEMF treatment, activation and phosphorylation of ERK1/2 were observed on day 1 and peaked on day 3. The expression level of p-ERK1/2 decreased on day 7 and 10. Expression level of p-p38 started low at day 1, kept increasing and reached highest level on day 7 and 10. After PEMF treatment, phosphorylation of ERK1/2 and p38 displayed a similar pattern as control group with continuous promoting of p-p38 and inhibition of p-ERK1/2.

To further validate the involvement of ERK and p38-MAPK pathways, pharmacological inhibition of ERK and p38 was given to hBMSCs pellets during chondrogenic induction and PEMF treatments. qPCR was performed to investigate the expression level of chondrogenic and hypertrophic markers after ERK and p38 inhibition at both early (day 3) and late (day 14) stage of MSCs chondrogenic differentiation (Fig. 5 g). In control group on day 3, inhibition of ERK1/2 led to increasing expression of *Sox9* and *RUNX2*, and inhibition of p38 resulted in downregulation of *Sox9* expression and upregulation of Runx2. On day 14, expression of *Sox9* was increased by ERK1/2 inhibition, and decreased by p38 inhibition, and expression of *RUNX2* was decreased by

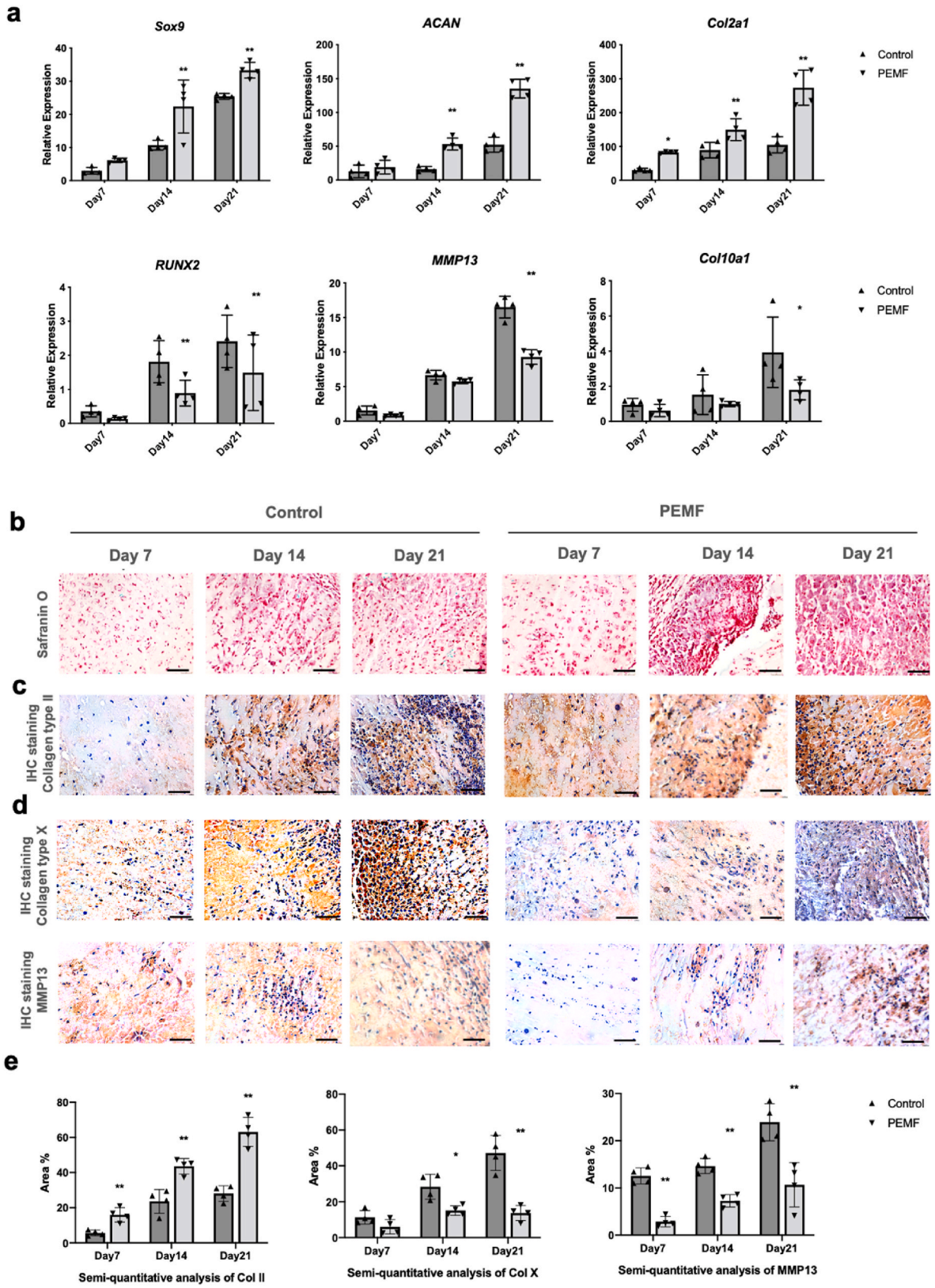

Fig. 3. PEMF affected RNA expression and matrix formation of rBMSCs during chondrogenic differentiation in hydrogels *in vitro*. a. qPCR analysis results showed that compared to control group, PEMF significantly upregulated the expressions of chondrogenic mRNA, and downregulated the expressions of hypertrophic mRNA. Staining of Safranin O (b) and immunohistochemistry of Col II (c, e) demonstrated that after PEMF treatment, significantly larger amounts of aggrecan and Col II were deposited in hydrogels. Immunohistochemistry of Col X and MMP13 (d, e) demonstrated that PEMF treatment could significantly inhibit the formation of hypertrophic proteins, revealing its chondro-protective potential. Scale bar: 50 μm *$p < 0.05$ **$p < 0.01$.

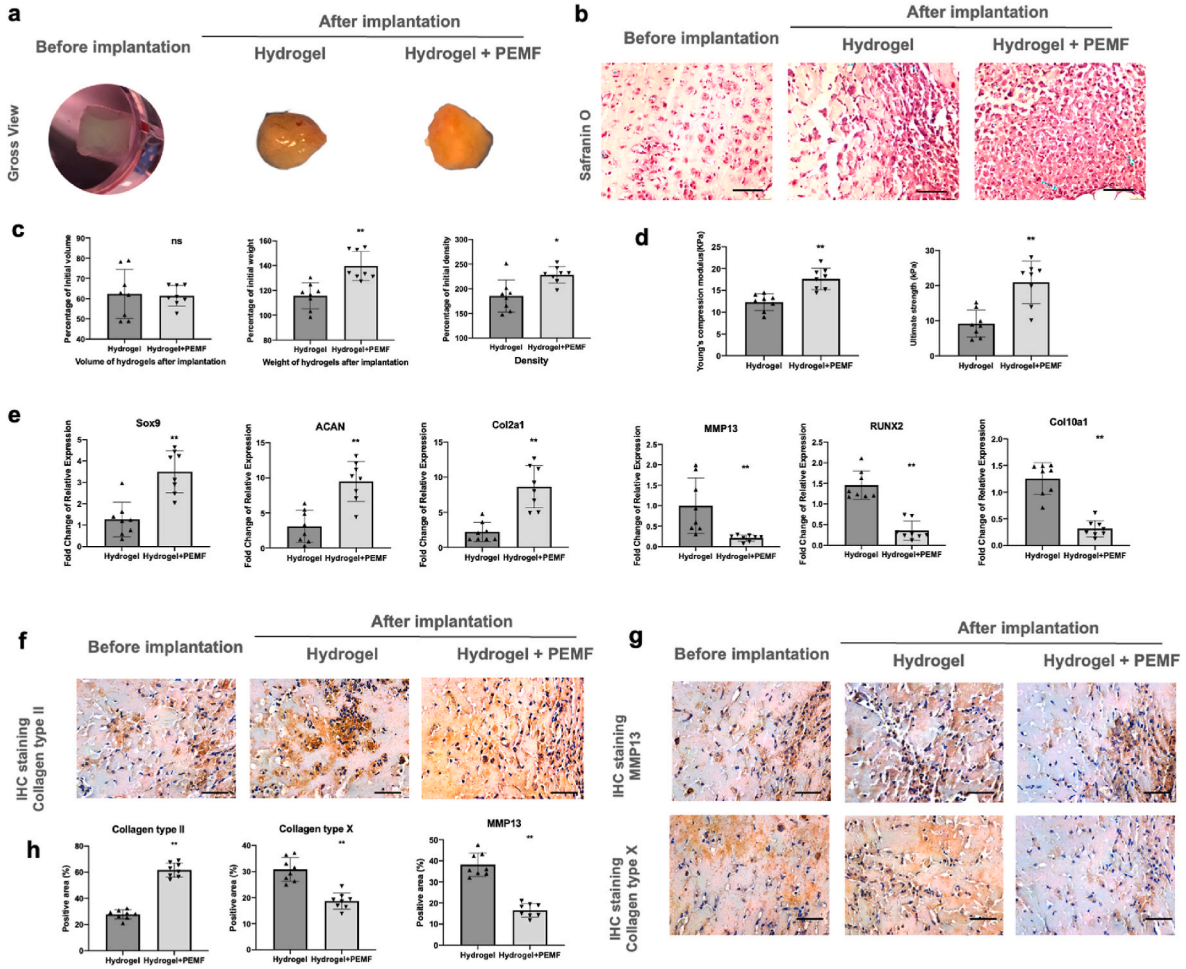

Fig. 4. PEMF promoted rBMSCs chondrogenesis in vivo. a Gross view of hydrogels before and after implantation. b afranin O staining of hydrogels after implantation. c Volume, weight, and density of hydrogels after implantation. d Mechanical property of hydrogels after implantation via compression test. e qPCR analysis of chondrogenic marker genes (*Sox9*, *ACAN* and *Col2a1*) and hypertrophic marker genes (*MMP13*, *RUNX2* and *Col10a1*). f IHC staining of Col II. g IHC staining of MMP13 and Col X. h Semi-quantitative analysis of IHC staining. n = 8/group. Scale bar: 50 μm *p < 0.05 **p < 0.01.

ERK1/2 inhibition, and increased by p38 inhibition. In PEMF group, inhibition of p38 resulted in dramatic downregulation of *Sox9* expression on both day 3 and 14, which showed no significant difference compared with control group, indicating that PEMF treatment promoted chondrogenesis of hBMSCs via upregulating the expression and phosphorylation of p38 and mediating p38 MAPK signaling pathway. Inhibition of ERK1/2 resulted in upregulation on day 3 and downregulation on day 14 of *RUNX2* expression, which showed no significant difference compared with control group treated with SB203580, indicating that ERK pathway might be involved in the inhibiting effects of PEMF on hypertrophic markers.

3.8. Healing outcomes of cartilage defects

H&E, safranin O and IHC staining (Fig. 6) were performed after 8 weeks of surgery. H&E results demonstrated that most of the hydrogels were dispersed and mostly degraded (Fig. 6 b). The residual hydrogels were surrounded by bony tissues under the newly formed cartilage. Samples from blank and MSCs groups only contained a layer of fibrous tissue with large amount of collagen type I but few collagen type II formation on the surface of defect site (Fig. 6 d, e). In the P-MSCs group, larger amounts of fibrocartilage-like tissue were observed on the surface of defect site. IHC staining demonstrated that the deposited matrix contained both collagen type I and II, confirming the regenerated cartilage to be mostly fibrocartilage. P-MSCs + PEMF group showed the best cartilage healing outcome with thicker layer of hyaline-like cartilage on the defect site. Hyaline chondrocytes were observed in regenerated cartilage surface according to histological staining, and the regenerated matrix on the surface was mostly collagen type II. Furthermore, IHC staining of collagen type X (Fig. 6 f, j) showed that much less collagen type X formation on the defect site were detected in P-MSCs + PEMF group compared to other groups, indicating that PEMF *in vivo* treatment provides chondroprotective effects against chondrocyte hypertrophy and cartilage degeneration. The quality of the cartilage regeneration is evaluated according to Wakitani scoring system [40]. (Fig. 6 g). P-MSCs + PEMF group achieved lowest score, demonstrating the best healing outcomes of osteochondral defect. Rats from P-MSCs group were scored significantly lower than blank and MSCs groups, indicating that PEMF enhanced engineered constructs are more beneficial for cartilage and subchondral bone repair. P-MSCs + PEMF group achieved better healing outcomes than P-MSCs group, indicating that PEMF *in vivo* treatment also enhanced cartilage regeneration.

4. Discussion

In this study, Alg-DA/Ac-β-CD/gelatin hydrogels based on chemical and physical multiple crosslinking and interactions strategy were successfully prepared. After confirming the effect of PEMF signals on rBMSCs chondrogenesis in our hydrogel system both *in vitro* and *in vivo*, we demonstrated the therapeutic potential of PEMF on enhancing

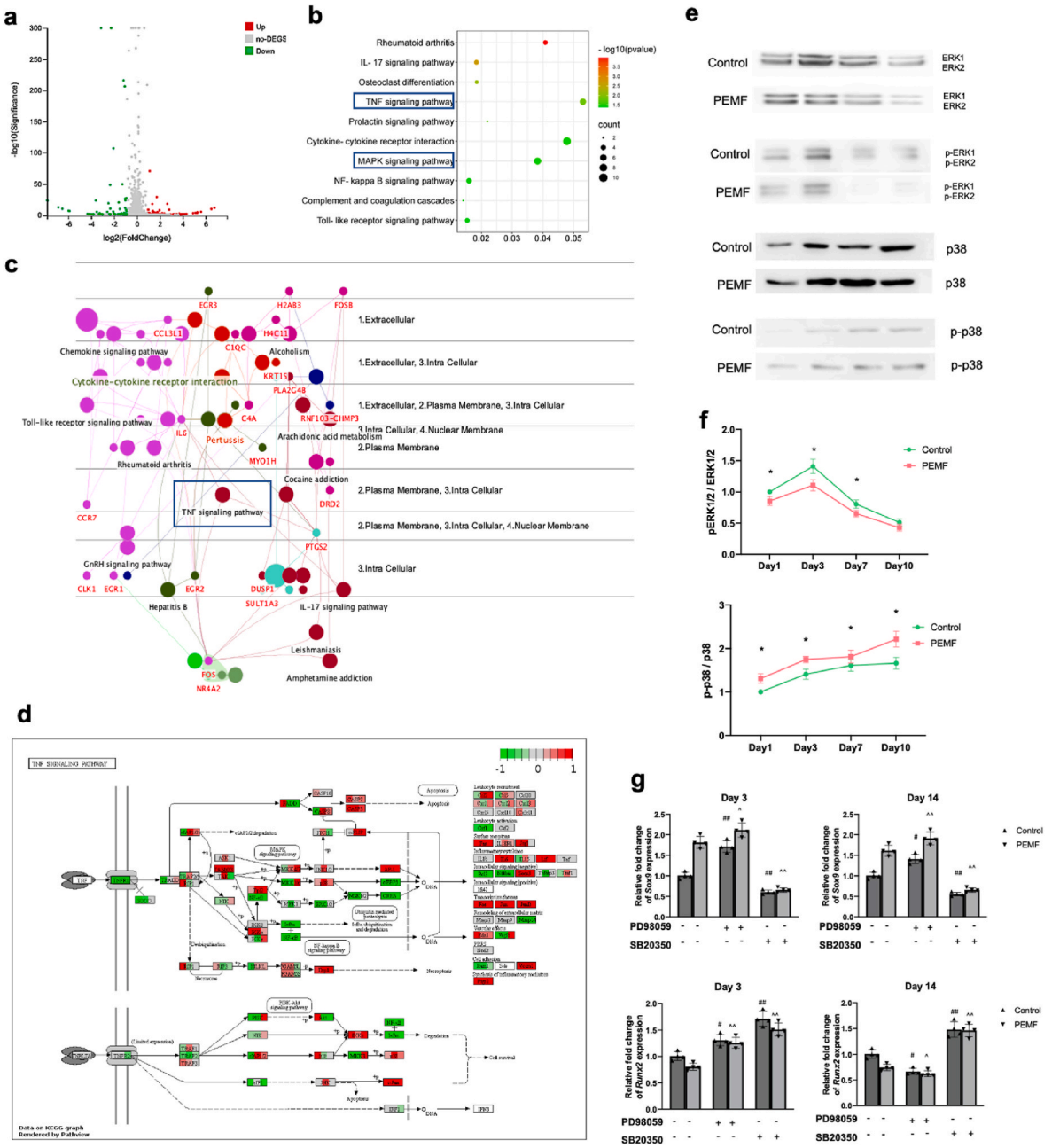

Fig. 5. RNA-seq analysis and validation study results. a Volcano plot of control-vs-PEMF revealing up- and down-regulated DEGs after PEMF treatment. b KEGG analysis of DEGs. c Gene-pathway interactions visualized in Cerebral Layout using ClueGo. d Gene expression changes of cells from three individual donors visualized in KEGG pathview of TNF-α pathway. e Protein expression levels of ERK1/2, p-ERK1/2, p38, and p-p38 were analyzed by Western blot. f Semi-quantitative analysis of each band was analyzed by ImageJ, and band intensity ratio ($A_{p\text{-}ERK}/A_{ERK}$ and $A_{p\text{-}p38}/A_{p38}$) were calculated (n = 4/group/time point). g Expression of chondrogenic marker (*Sox9*) and hypertrophic marker (*Runx2*) in hBMSCs during chondrogenic induction after ERK1 / 2 and p38 inhibition on day 3 and 14 (n = 4/group/time point). *p < 0.05 **p < 0.01. # vs control group without inhibition, ^ vs PEMF group without inhibition, #, ^ p < 0.05, ##, ^^ p < 0.01.

cartilage repair in combination of MSCs-based tissue engineering using a rat osteochondral defect model.

Suitable scaffolds are essential for cartilage tissue engineering. In our study, we successfully designed a convenient approach to produce supramolecular hydrogels of desirable attributes via chemical and physical multiple crosslinking and interactions strategy, and thereby introduced stronger and more suitable physical properties for hydrogels in cartilage repair. Our study demonstrated that our hydrogels presented injectable, re-moldable and ideal mechanical properties. Furthermore, owing to the enhanced physical properties brought by chemical and physical multiple crosslinking and interactions, our hydrogels showed relative low swelling ratio, appropriate degradation rate, and tissue adhesive abilities, and have an impact on the availability of implanted hydrogels and benefit their biomedical applications.

3,4-dihydroxyphenethylamine, also called dopamine (DA), which contains catechol group, is a neuromodulatory molecule and exhibit favorable biocompatibility and high adhesive property [43]. DA was often utilized in tissue engineering researches because it showed ideal interactions with tissues via hydrogen bonds and covalent bonds [44]. Therefore, introduction of DA would introduce multiple interactions to the hydrogel system and help to keep the implanted hydrogel stable in the defected tissues.

In our hydrogel system, reversible linkage of the host-guest interactions and chemically crosslinked acrylated structure were the main

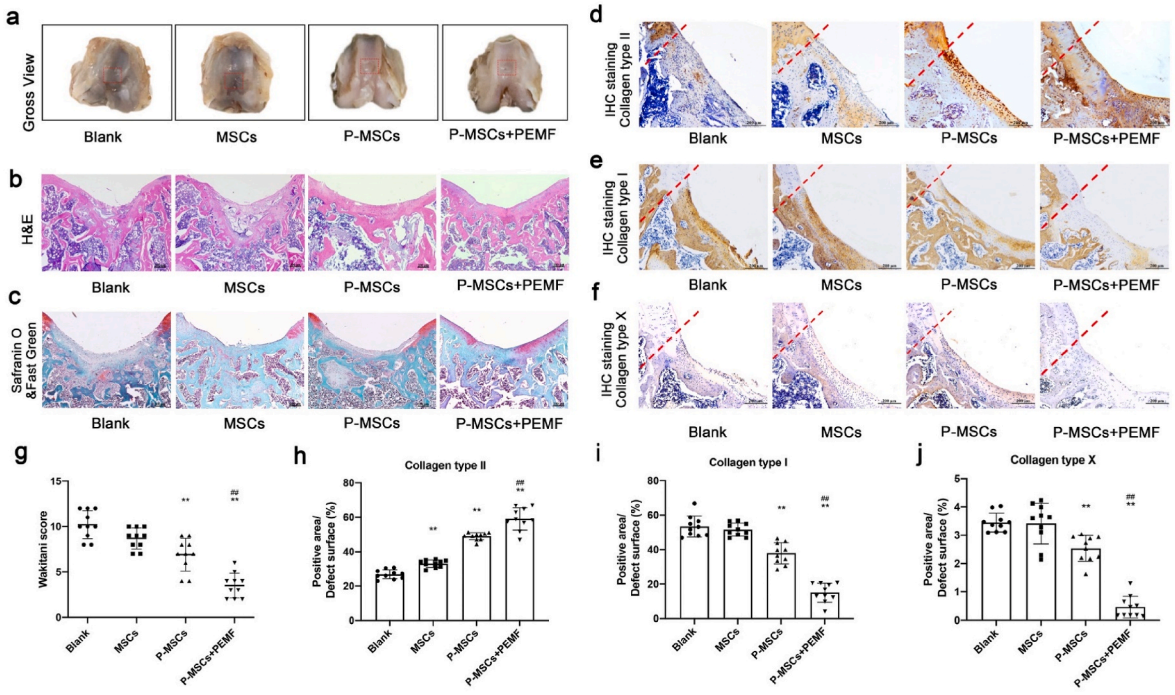

Fig. 6. PEMF treatment promoted cartilage defect healing in rat osteochondral defect model.
a Macroscopic appearance of the rat osteochondral defect. **b** H&E staining of the rat osteochondral defect sections. **c** Safranin O & Fast Green staining of the rat osteochondral defect sections. **d** Immunohistochemical staining of type II collagen. **e** Immunohistochemical staining of type I collagen. **f** Immunohistochemical staining of type X collagen. **g** Cartilage regeneration evaluated by the Wakitani scoring system at week 8 after surgery. **h-j** Semi-quantitative analysis of IHC staining of collagen type II, I and X. *p < 0.05 vs. blank group, **p < 0.01 vs. blank group, ##p < 0.01 vs P-MSCs group. n = 10/group/time point.

structure. With the modification of dopamine, hydrogen bonds and π-π interactions would be introduced into the hydrogel system. But the introduced interactions would not affect the polymerization of double bonds in Ac-β-CD. The aromatic rings of catechol groups could exhibit absorption under 280 nm. But in our hydrogel system, 365 nm of UV light was utilized to initiate the polymerization. Thus, the influence of catechol groups would not be obvious.

It is worth noting that during hydrogel preparation, there is a pre-gel state where increased viscosity was observed. In this state, the pre-gel is in semi-solid form and can be either administrated in situ and then crosslinked, or pre-formed *in vitro* and injected to the target site, which brought out more translational value to our hydrogel system. This feature grants multiple administration pathways to our hydrogel system, which makes it more practical and can be involved in much more complex biomedical application scenarios. Furthermore, our study demonstrated that the modified hydrogels revealed suitable biological properties such as supporting encapsulated cells, allowing molecular transportation and facilitating matrix deposition. Large scale of cell aggregation was observed in our hydrogels *in vitro* and *in vivo*, indicating the reversible nature of our hydrogels supports cell migration, which benefited chondrogenesis of MSCs. After transplanted into rat osteochondral defect site, the desirable properties of our hydrogels led to desirable outcomes of subchondral bone healing and cartilage-bone junction formation.

Adult articular cartilage exhibits little capacity for intrinsic repair, and cartilage tissue engineering remains the most promising strategy for the successful repair of articular cartilage defects. By manipulating cells, scaffolds, and stimuli, tissue engineering promised healing of damaged tissues and organs via the use of living, functional constructs [45]. Cartilage, with homogeneous structure and few cell types, was originally recognized as one of the first targets of tissue engineering [46]. However, the complex requirement for cartilage regeneration led the healing of cartilage defects to be elusive. In MSCs-based tissue engineering strategies, the chondro-differentiation ability of MSCs was predicted to fulfill the desired criteria for cartilage regeneration. However, apart from chondrocytes, MSCs can also differentiate into other cell types including fibrochondrocytes and hypertrophic chondrocytes, resulting in a mixture of cartilaginous, fibrous, and hypertrophic tissues [19,20]. *In vitro* chondro-induction of MSCs also results in an unnatural differentiation with co-expression of hyaline cartilage markers (collagen type II and SOX-9) and hypertrophic markers (collagen type X and MMP13) [47]. The success of MSC-based techniques may remain limited if the presence of fibrous and hypertrophic tissue cannot be eliminated [46]. Therefore, in our study, PEMF treatment revealed great therapeutic potential, as it could not only promote chondro-differentiation of MSCs, but also inhibit the expression of hypertrophic markers during chondro-induction, thus enhancing the quality of tissue engineered constructs. Applying PEMF *in vivo* could also mitigate the hypertrophic process, and facilitate the in situ regeneration of hyaline-like cartilage in osteochondral defects. The effects of PEMF on chondrocytes and MSCs chondrogenic differentiation have been studied, and most of the studies reported the positive effects. The beneficial effects of PEMF on cartilage cells include promoting proliferation, increasing anabolic activities, and antagonizing the catabolic effects of inflammation [22–24]. PEMF treatment affected anabolic activities through upregulating the expression of chondrogenic markers and increasing synthesis of cartilage extracellular matrix (ECM) components, such as GAG and type II collagen [48]. PEMF exposure decreased the pro-inflammatory cytokine release such as interleukin (IL)-6 and IL-8 [25]. Several studies have confirmed the promoting effects of PEMF on MSCs chondrogenic differentiation [49–52]. When exposed to PEMF, type II collagen and glycosaminoglycan (GAG) synthesis were increased in MSCs, indicating that PEMF was able to stimulate and maintain chondrogenesis of MSCs [51]. PEMF exposure during chondrogenic differentiation inhibited the catabolic effects induced by IL-1β, suggesting that PEMF may help to improve clinical outcome in cartilage tissue engineering [53]. More recently, Stefani et al. demonstrated that PEMF exposure could enhance the quality of tissue-engineered cartilage grafts, and therefore promote

engineered cartilage growth and repair [54].

Despite the promising potentials of PEMF that have been reported in chondrogenesis and cartilage repair, the effects of PEMF were believed to be signal specific [55]. Therefore, experimental and clinical studies are still needed to understand the optimal PEMF signal and mechanisms for a defined specific condition. In our study, we used a specific PEMF signal which revealed superior beneficial effects on BMSCs chondrogenesis and cartilage repair. PEMF treatment via this signal promoted rBMSCs chondrogenesis and slowed down cell hypertrophy, indicating its potential to enhance the quality of engineered construct during *in vitro* preparation. In rat osteochondral defect models, PEMF treatment demonstrated promising therapeutic potential on cartilage repair, and combining with chondrogenic induced MSCs-laden hydrogels, better outcome of cartilage healing was achieved. Through bioinformatic analysis and the following mechanism study, we also demonstrated that our PEMF signal promoted chondrogenesis via upregulating the expression and phosphorylation of p38, and inhibiting hypertrophic markers expression via ERK pathway. These findings suggested that our PEMF signal revealed superior potential in cartilage repair, providing a potential low-cost, low-risk, noninvasive treatment modality to augment the therapeutic effects of cartilage tissue engineering.

In musculoskeletal system, tissues and cells were found sensitive to biophysical stimulations. The diamond concept [21] was thereby proposed to underpin tissue engineering, which introduced environmental biophysical stimulation as the 4th key element apart from cells, scaffolds, growth factor/cytokines. In comparison to other biophysical stimulations, such as mechanical loading and low intensity pulsed ultrasound (LIPUS), PEMF offers unique advantages as a non-contact, non-invasive stimulation. Furthermore, compared to optical, acoustic, and electrical fields as well as mechanical forces, electromagnetic fields have advantages because of their large force output, high precision, and deep tissue penetration [56]. During tissue engineered constructs preparation *in vitro*, PEMF treatment offers chondro-inductive effects without any increased risk of contamination. As for clinical treatments, since PEMF have been successfully employed as adjunctive therapy for the treatment of many orthopaedics conditions [57–59], numerous types of portable devices were developed, which is suitable for treatment in hospital and physiotherapy from home. This makes PEMF safer and more convenient to use compared to other physical treatments, which is more practical in clinical situations. We therefore consider PEMF to be a perfect candidate as physical stimulation to complete the diamond concept.

Despite our encouraging findings which could lead credence to clinical application, there are limitations in the current study. Firstly, daily PEMF treatment (3 h/day) was given according to our previous studies [32,60]. The dose–response of PEMF treatment *in vitro* and *in vivo* was not investigated. Secondly, the parameters of PEMF signal were not investigated in this study, comparison of different PEMF signals might help us further explore more therapeutic signals and understand how PEMFs work and their underlying mechanisms. Future research endeavors should focus on these studies, in order to explore more practical tissue engineering strategies for clinical applications.

5. Conclusion

The chemical structure, injectability, self-healing behavior, morphology, swelling behavior, adhesiveness, *in vitro/in vivo* biocompatibility, and therapeutic efficacy for cartilage repair of the Alg-DA/Ac-β-CD/gelatin hydrogels were systematically characterized. All of the results suggested that the injectable self-healing adhesive hydrogel exhibit ideal properties for cartilage engineering. PEMF signal promoted BMSCs chondrogenesis and inhibited hypertrophic processes, and thereby enhanced the quality of engineered chondrogenic constructs. Together with enhanced chondrogenic constructs induced from BMSCs laden hydrogels, PEMF promoted cartilage healing in rat osteochondral defect models, and demonstrated great potential as 4th element in cartilage tissue engineering and translational value in clinical applications.

CRediT authorship contribution statement

Yucong Li: Conceptualization, Data curation, Formal analysis, Investigation, Methodology, Project administration, Roles/Writing – original draft. **Linlong Li:** Data curation, Formal analysis, Investigation, Methodology, Roles/Writing – original draft. **Ye Li:** Data curation, Formal analysis, Investigation, Roles/Writing – original draft. **Lu Feng:** Investigation, Resources, Software. **Bin Wang:** Investigation, Resources, Software. **Ming Wang:** Investigation, Methodology. **Haixing Wang:** Investigation, Methodology. **Meiling Zhu:** Methodology. **Yongkang Yang:** Investigation. **Erik I. Waldorff:** Conceptualization, Funding acquisition. **Nianli Zhang:** Conceptualization, Funding acquisition. **Ingmar Viohl:** Resources, Funding acquisition. **Sien Lin:** Supervision, Validation, Writing – review & editing. **Liming Bian:** Supervision, Validation. **Wayne Yuk-Wai Lee:** Supervision, Validation, Writing – review & editing. **Gang Li:** Conceptualization, Funding acquisition, Project administration, Resources, Writing – review & editing.

Declaration of competing interest

The authors have no conflicts of interest to disclose in relation to this article. NZ, EIW and IV are employees of and own stock in Orthofix Medical Inc., USA.

Acknowledgements

This work was partially supported by grants from University Grants Committee, Research Grants Council of the Hong Kong Special Administrative Region, China (14108720, 14121721, 14202920, T13-402/17-N and AoE/M-402/20). This study also received support from the research funds from Health@InnoHK program launched by Innovation Technology Commission of the Hong Kong SAR, PR China. The authors would like to acknowledge Orthofix Medical Inc. USA for providing the PEMF devices, their technical and funding support for this study.

Appendix A. Supplementary data

Supplementary data to this article can be found online at https://doi.org/10.1016/j.bioactmat.2022.10.010.

References

[1] T.A. Holland, J.K. Tessmar, Y. Tabata, A.G. Mikos, Transforming growth factor-β1 release from oligo (poly (ethylene glycol) fumarate) hydrogels in conditions that model the cartilage wound healing environment, Journal of controlled release 94 (1) (2004) 101–114.

[2] Z. Man, X. Hu, Z. Liu, H. Huang, Q. Meng, X. Zhang, L. Dai, J. Zhang, X. Fu, X. Duan, Transplantation of allogenic chondrocytes with chitosan hydrogel-demineralized bone matrix hybrid scaffold to repair rabbit cartilage injury, Biomaterials 108 (2016) 157–167.

[3] D. Albani, A. Gloria, C. Giordano, S. Rodilossi, T. Russo, U. D'Amora, M. Tunesi, A. Cigada, L. Ambrosio, G. Forloni, Hydrogel-based nanocomposites and mesenchymal stem cells: a promising synergistic strategy for neurodegenerative disorders therapy, Sci. World J. 2013 (2013).

[4] J. Wang, F. Zhang, W.P. Tsang, C. Wan, C. Wu, Fabrication of injectable high strength hydrogel based on 4-arm star PEG for cartilage tissue engineering, Biomaterials 120 (2017) 11–21.

[5] M.F.P. Graca, S.P. Miguel, C.S.D. Cabral, I.J. Correia, Hyaluronic acid-Based wound dressings: a review, Carbohydr. Polym. 241 (2020).

[6] S. Hong, K. Yang, B. Kang, C. Lee, I.T. Song, E. Byun, K.I. Park, S.W. Cho, H. Lee, Hyaluronic acid catechol: a biopolymer exhibiting a pH-dependent adhesive or cohesive property for human neural stem cell engineering, Adv. Funct. Mater. 23 (14) (2013) 1774–1780.

[7] X.L. Li, A. Sigen, Q. Xu, F. Alshehri, M. Zeng, D.Z. Zhou, J. Li, G.Q. Zhou, W. X. Wang, Cartilage-Derived progenitor cell-laden injectable hydrogel-an approach for cartilage tissue regeneration, ACS Appl. Bio Mater. 3 (8) (2020) 4756–4765.

[8] A. Das, M. Abas, N. Biswas, P. Banerjee, N. Ghosh, A. Rawat, S. Khanna, S. Roy, C. K. Sen, A modified collagen dressing induces transition of inflammatory to reparative phenotype of wound macrophages, Sci. Rep. 9 (2019).

[9] H. Hamedi, S. Moradi, S.M. Hudson, A.E. Tonelli, Chitosan based hydrogels and their applications for drug delivery in wound dressings: a review, Carbohydr. Polym. 199 (2018) 445–460.

[10] L. Zhang, Y.N. Ma, X.C. Pan, S.Y. Chen, H.H. Zhuang, S.F. Wang, A composite hydrogel of chitosan/heparin/poly (gamma-glutamic acid) loaded with superoxide dismutase for wound healing, Carbohydr. Polym. 180 (2018) 168–174.

[11] K. Varaprasad, T. Jayaramudu, V. Kanikireddy, C. Toro, E.R. Sadiku, Alginate-based composite materials for wound dressing application:A mini review, Carbohydr. Polym. 236 (2020).

[12] X.L. Li, Q. Xu, M. Johnson, X. Wang, J. Lyu, Y.H. Li, S. McMahon, U. Greiser, A. Sigen, W.X. Wang, A chondroitin sulfate based injectable hydrogel for delivery of stem cells in cartilage regeneration, Biomater Sci-Uk 9 (11) (2021) 4139–4148.

[13] Q. Feng, K.C. Wei, S.E. Lin, Z. Xu, Y.X. Sun, P. Shi, G. Li, L.M. Bian, Mechanically resilient, injectable, and bioadhesive supramolecular gelatin hydrogels crosslinked by weak host-guest interactions assist cell infiltration and in situ tissue regeneration, Biomaterials 101 (2016) 217–228.

[14] Z.X. Bai, W.H. Dan, G.F. Yu, Y.J. Wang, Y.N. Chen, Y.P. Huang, C.K. Yang, N. H. Dan, Tough and tissue-adhesive polyacrylamide/collagen hydrogel with dopamine-grafted oxidized sodium alginate as crosslinker for cutaneous wound healing, RSC Adv. 8 (73) (2018) 42123–42132.

[15] J. Li, A.D. Celiz, J. Yang, Q. Yang, I. Wamala, W. Whyte, B.R. Seo, N.V. Vasilyev, J. J. Vlassak, Z. Suo, D.J. Mooney, Tough adhesives for diverse wet surfaces, Science 357 (6349) (2017) 378–381.

[16] W. Wei, Y.Z. Ma, X.D. Yao, W.Y. Zhou, X.Z. Wang, C.L. Li, J.X. Lin, Q.L. He, S. Leptihn, H.W. Ouyang, Advanced hydrogels for the repair of cartilage defects and regeneration, Bioact. Mater. 6 (4) (2021) 998–1011.

[17] Y.L. Yang, J.Y. Zhang, Z.Z. Liu, Q.N. Lin, X.L. Liu, C.Y. Bao, Y. Wang, L.Y. Zhu, Tissue-integratable and biocompatible photogelation by the imine crosslinking reaction, Adv. Mater. 28 (14) (2016) 2724–2730.

[18] J.M. Lee, M.T. Sultan, S.H. Kim, V. Kumar, Y.K. Yeon, O.J. Lee, C.H. Park, Artificial auricular cartilage using silk fibroin and polyvinyl alcohol hydrogel, Int. J. Mol. Sci. 18 (8) (2017) 1707.

[19] K. Mithoefer, T. McAdams, R.J. Williams, P.C. Kreuz, B.R. Mandelbaum, Clinical efficacy of the microfracture technique for articular cartilage repair in the knee: an evidence-based systematic analysis, Am. J. Sports Med. 37 (10) (2009) 2053–2063.

[20] E. Steck, J. Fischer, H. Lorenz, T. Gotterbarm, M. Jung, W. Richter, Mesenchymal stem cell differentiation in an experimental cartilage defect: restriction of hypertrophy to bone-close neocartilage, Stem Cell. Dev. 18 (7) (2009) 969–978.

[21] P.V. Giannoudis, T.A. Einhorn, D. Marsh, Fracture healing: the diamond concept, Injury 38 (2007) S3–S6.

[22] C.H. Chang, S.T. Loo, H.L. Liu, H.W. Fang, H.Y. Lin, Can low frequency electromagnetic field help cartilage tissue engineering? J. Biomed. Mater. Res. Part A: An Official Journal of The Society for Biomaterials, The Japanese Society for Biomaterials, and The Australian Society for Biomaterials and the Korean Society for Biomaterials 92 (3) (2010) 843–851.

[23] M.D. Mattei, A. Caruso, F. Pezzetti, A. Pellati, G. Stabellini, V. Sollazzo, G. C. Traina, Effects of pulsed electromagnetic fields on human articular chondrocyte proliferation, Connect. Tissue Res. 42 (4) (2001) 269–279.

[24] S. Anbarasan, U. Baraneedharan, S.F. Paul, H. Kaur, S. Rangaswami, E. Bhaskar, Low dose short duration pulsed electromagnetic field effects on cultured human chondrocytes: an experimental study, Indian J. Orthop. 50 (1) (2016) 87.

[25] F. Vincenzi, M. Targa, C. Corciulo, S. Gessi, S. Merighi, S. Setti, R. Cadossi, M. B. Goldring, P.A. Borea, K. Varani, Pulsed electromagnetic fields increased the anti-inflammatory effect of A2A and A3 adenosine receptors in human T/C-28a2 chondrocytes and hFOB 1.19 osteoblasts, PLoS One 8 (5) (2013).

[26] M. Fini, G. Giavaresi, P. Torricelli, F. Cavani, S. Setti, V. Canè, R. Giardino, Pulsed electromagnetic fields reduce knee osteoarthritic lesion progression in the aged Dunkin Hartley Guinea pig, J. Orthop. Res. 23 (4) (2005) 899–908.

[27] M. Fini, P. Torricelli, G. Giavaresi, N.N. Aldini, F. Cavani, S. Setti, A. Nicolini, A. Carpi, R. Giardino, Effect of pulsed electromagnetic field stimulation on knee cartilage, subchondral and epyphiseal trabecular bone of aged Dunkin Hartley Guinea pigs, Biomed. Pharmacother. 62 (10) (2008) 709–715.

[28] D.M. Ciombor, R. Aaron, S. Wang, B. Simon, Modification of osteoarthritis by pulsed electromagnetic field—a morphological study, Osteoarthritis Cartilage 11 (6) (2003) 455–462.

[29] F. Benazzo, M. Cadossi, F. Cavani, M. Fini, G. Giavaresi, S. Setti, R. Cadossi, R. Giardino, Cartilage repair with osteochondral autografts in sheep: effect of biophysical stimulation with pulsed electromagnetic fields, J. Orthop. Res. 26 (5) (2008) 631–642.

[30] W.Y. Lee, W.-l. Tse, P.-c. Ho, C.W.-y. Wong, Y.-Y. Kwok, G. Li, Phase I Clinical Trial of Intra-articular Injection of Autologous Mesenchymal Stem Cells for the Treatment of Wrist Chondral Defect.

[31] C. Lee, J. Shin, J.S. Lee, E. Byun, J.H. Ryu, S.H. Um, D.I. Kim, H. Lee, S.W. Cho, Bioinspired, calcium-free alginate hydrogels with tunable physical and mechanical properties and improved biocompatibility, Biomacromolecules 14 (6) (2013) 2004–2013.

[32] Y. Li, Y. Yang, M. Wang, X. Zhang, S. Bai, X. Lu, Y. Li, E.I. Waldorff, N. Zhang, W.Y.-W. Lee, G. Li, High slew rate pulsed electromagnetic field enhances bone consolidation and shortens daily treatment duration in distraction osteogenesis, Bone Joint Res. 10 (12) (2021) 767–779.

[33] D.E. Garland, B. Moses, W. Salyer, Long-term follow-up of fracture nonunions treated with PEMFs, Contemp. Orthop. 22 (3) (1991) 295–302.

[34] M. Wang, Y. Li, L. Feng, X. Zhang, H. Wang, N. Zhang, I. Viohl, G. Li, Pulsed electromagnetic field enhances healing of a meniscal tear and mitigates posttraumatic osteoarthritis in a rat model, Am. J. Sports Med. 50 (10) (2022) 2722–2732.

[35] Y. Liu, J. Xu, L. Xu, T. Wu, Y. Sun, Y.W. Lee, B. Wang, H.C. Chan, X. Jiang, J. Zhang, Cystic fibrosis transmembrane conductance regulator mediates tenogenic differentiation of tendon-derived stem cells and tendon repair: accelerating tendon injury healing by intervening in its downstream signaling, Faseb. J. 31 (9) (2017) 3800–3815.

[36] L. Wang, Z. Feng, X. Wang, X. Wang, X. Zhang, DEGseq: an R package for identifying differentially expressed genes from RNA-seq data, Bioinformatics 26 (1) (2010) 136–138.

[37] R.L. Dahlin, L.A. Kinard, J. Lam, C.J. Needham, S. Lu, F.K. Kasper, A.G. Mikos, Articular chondrocytes and mesenchymal stem cells seeded on biodegradable scaffolds for the repair of cartilage in a rat osteochondral defect model, Biomaterials 35 (26) (2014) 7460–7469.

[38] N. Tran-Khanh, C.D. Hoemann, M.D. McKee, J.E. Henderson, M.D. Buschmann, Aged bovine chondrocytes display a diminished capacity to produce a collagen-rich, mechanically functional cartilage extracellular matrix, J. Orthop. Res. 23 (6) (2005) 1354–1362.

[39] Y. Chen, Y. Sun, X. Pan, K. Ho, G. Li, Joint distraction attenuates osteoarthritis by reducing secondary inflammation, cartilage degeneration and subchondral bone aberrant change, Osteoarthritis Cartilage 23 (10) (2015) 1728–1735.

[40] S. Wakitani, T. Goto, S.J. Pineda, R.G. Young, J.M. Mansour, A.I. Caplan, V. M. Goldberg, Mesenchymal cell-based repair of large, full-thickness defects of articular cartilage, the Journal of bone and joint surgery, Am. Vol. 76 (4) (1994) 579–592.

[41] W. Luo, C. Brouwer, Pathview: an R/Bioconductor package for pathway-based data integration and visualization, Bioinformatics 29 (14) (2013) 1830–1831.

[42] W. Luo, G. Pant, Y.K. Bhavnasi, S.G. Blanchard Jr., C. Brouwer, Pathview Web: user friendly pathway visualization and data integration, Nucleic Acids Res. 45 (W1) (2017) W501–W508.

[43] H. Lee, S.M. Dellatore, W.M. Miller, P.B. Messersmith, Mussel-inspired surface chemistry for multifunctional coatings, Science 318 (5849) (2007) 426–430.

[44] S. Moulay, Dopa/catechol-tethered polymers: bioadhesives and biomimetic adhesive materials, Polym. Rev. 54 (3) (2014) 436–513.

[45] R. Langer, J.P. Vacanti, Tissue engineering, Science 260 (5110) (1993) 920–926.

[46] D.J. Huey, J.C. Hu, K.A. Athanasiou, Unlike bone, cartilage regeneration remains elusive, Science 338 (6109) (2012) 917–921.

[47] K. Pelttari, A. Winter, E. Steck, K. Goetzke, T. Hennig, B.G. Ochs, T. Aigner, W. Richter, Premature induction of hypertrophy during in vitro chondrogenesis of human mesenchymal stem cells correlates with calcification and vascular invasion after ectopic transplantation in SCID mice, Arthritis Rheum.: Off. J. Am. College Rheumatol. 54 (10) (2006) 3254–3266.

[48] S.H. Chang, Y.W. Hsiao, H.Y. Lin, Low-frequency electromagnetic field exposure accelerates chondrocytic phenotype expression on chitosan substrate, Orthopedics 34 (1) (2011), 20-20.

[49] M. Esposito, A. Lucariello, C. Costanzo, A. Fiumarella, A. Giannini, G. Riccardi, I. Riccio, Differentiation of human umbilical cord-derived mesenchymal stem cells, WJ-MSCs, into chondrogenic cells in the presence of pulsed electromagnetic fields, In Vivo 27 (4) (2013) 495–500.

[50] C.-H. Chen, Y.-S. Lin, Y.-C. Fu, C.-K. Wang, S.-C. Wu, G.-J. Wang, R. Eswaramoorthy, Y.-H. Wang, C.-Z. Wang, Y.-H. Wang, Electromagnetic fields enhance chondrogenesis of human adipose-derived stem cells in a chondrogenic microenvironment in vitro, J. Appl. Physiol. 114 (5) (2013) 647–655.

[51] S. Mayer-Wagner, A. Passberger, B. Sievers, J. Aigner, B. Summer, T.S. Schiergens, V. Jansson, P.E. Müller, Effects of low frequency electromagnetic fields on the chondrogenic differentiation of human mesenchymal stem cells, Bioelectromagnetics 32 (4) (2011) 283–290.

[52] E. Vinod, U. Kachroo, G. Rebekah, S. Thomas, B. Ramasamy, In vitro chondrogenic differentiation of human articular cartilage derived chondroprogenitors using pulsed electromagnetic field, J. Clin. Orthopaedics Trauma 14 (2021) 22–28.

[53] A. Ongaro, A. Pellati, S. Setti, F.F. Masieri, G. Aquila, M. Fini, A. Caruso, M. De Mattei, Electromagnetic fields counteract IL-1β activity during chondrogenesis of bovine mesenchymal stem cells, J. Tissue Eng. Regen. Med. 9 (12) (2015) E229–E238.

[54] R.M. Stefani, S. Barbosa, A.R. Tan, S. Setti, A.M. Stoker, G.A. Ateshian, R. Cadossi, G. Vunjak-Novakovic, R.K. Aaron, J.L. Cook, Pulsed electromagnetic fields promote repair of focal articular cartilage defects with engineered osteochondral constructs, Biotechnol. Bioeng. 117 (5) (2020) 1584–1596.

[55] E.I. Waldorff, N. Zhang, J.T. Ryaby, Pulsed electromagnetic field applications: a corporate perspective, J. Orthop. Trans. 9 (2017) 60–68.

[56] X. Wang, J. Law, M. Luo, Z. Gong, J. Yu, W. Tang, Z. Zhang, X. Mei, Z. Huang, L. You, Magnetic measurement and stimulation of cellular and intracellular structures, ACS Nano 14 (4) (2020) 3805–3821.

[57] C. Andrew, L. Bassett, R.J. Pawluk, A.A. Pilla, Augmentation of bone repair by inductively coupled electromagnetic fields, Science 184 (4136) (1974) 575–577.

[58] C. Faldini, M. Cadossi, D. Luciani, E. Betti, E. Chiarello, S. Giannini, Electromagnetic bone growth stimulation in patients with femoral neck fractures treated with screws: prospective randomized double-blind study, Curr. Orthopaedic Pract. 21 (3) (2010) 282–287.

[59] A. Martinez-Rondanelli, J.P. Martinez, M.E. Moncada, E. Manzi, C.R. Pinedo, H. Cadavid, Electromagnetic stimulation as coadjuvant in the healing of diaphyseal femoral fractures: a randomized controlled trial, Colomb. Méd. 45 (2) (2014) 67–71.

[60] Y. Li, Q. Pan, N. Zhang, B. Wang, Z. Yang, J.T. Ryaby, E.I. Waldorff, W.Y.-W. Lee, G. Li, A novel pulsed electromagnetic field promotes distraction osteogenesis via enhancing osteogenesis and angiogenesis in a rat model, J. Orthopaedic Trans. 25 (2020) 87–95.